FBK Optical Data Association in a Multi-Hypothesis Framework with Maneuvers

W. R. Faber and Islam I. Hussein
Applied Defense Solutions
John T. Kent and Shambo Bhattacharjee
University of Leeds
Moriba K. Jah
University of Texas at Austin

ABSTRACT

In Space Situational Awareness (SSA), one may encounter scenarios where the measurements received at a certain time do not correlate to a known Resident Space Object (RSO). Without information that uniquely assigns the measurement to a particular RSO there can be no certainty on the identity of the object. It could bethatthemeasurementwasproducedbyclutterorperhapsanewlybirthedRSO. It is also a possibility that the measurement came from a previously known object that maneuvered away from its predicted location. Typically, tracking methods tend to associate uncorrelated measurements to new objects and wait for more information to determine the true RSO population. This can lead to the loss of object custody. The goal of this paper is to utilize a multiple hypothesis framework coupled with some knowledge of RSO maneuvers that allows the user to maintain object custody in scenarios with uncorrelated optical measurement returns. This is achieved by fitting a Fisher-Bingham-Kent type distribution to the hypothesized maneuvers for accurate data association using directional discriminant analysis.

1. INTRODUCTION

In previous work, we introduce the idea of using the Fisher-Bingham-Kent (FBK) distribution to distinguish between data association ambiguities of maneuvering objects [1]. We did this by converting a particle representation of the object pdf to an FBK distribution and then used discriminant analysis and the tail probability to determine probable associations. The overall goal of this work is to show the capability of maintaining custody of maneuvering Resident Space Object (RSO). In practice, custody can be lost when data providers are unaware of a change in the tracked RSO's dynamics. Changes occur when objects are maneuvered or when unmodeled forces are applied to the RSO. These changes are often accompanied by various uncertainties; for example, in the directions of the applied forces, in the magnitudes of the applied forces, and in the start time and duration of the maneuver. These uncertainties accumulate to a large uncertainty in the object's final state. When coupled with the fact that many maneuvers are possible at any given moment the prediction and tracking of maneuvers can become computationally expensive. In this paper, we expand previous work to formally introduce the use of the FBK within a multiple hypothesis framework. The family of FBK distributions, provided by Kent et al. [2], and their utility in providing accurate data association was discussed in [3]. This topic is explored in the paradigm of optical angles-only measurements. In directional discriminant analysis was presented to distinguish between optical angles-only data association ambiguities in an Observation to Track Association (OTTA) problem. Applying similar techniques to maneuvered object probability density function (PDF) can discriminate between maneuver types. Over the past few decades the SSA community has looked at a variety of solutions to the maneuvering object problem. One approach that has drawn interest is the Interactive Multiple Model (IMM) and its variations for tracking maneuvering objects. An IMM is a way to incorporate different dynamic models for an object in order to better account for unknown dynamics. Typically, in the SSA community, multiple models with different process noise levels are used to discriminate between maneuvers. Different variations of the IMM stem from the underlying filter used to perform updates. This is seen in work by Jia et al. [4] and Chen et al. [5] where IMM is used with Cubature Kalman Filter (CKF) and Joint Probability Data Association Filter (JPDAF) respectively. Other noteworthy techniques are those that incorporate historical data to perform post-maneuver observation correlation as in J.A. Siminski et al. [6]

In this paper, we implement the FBK into a full multiple hypothesis framework called Randomized Finite Set Statistics (R-FISST) [7]. In doing so we maintain object custody through a maneuver. We use multiple previously known dynamic models to represent possible space object maneuvers similar to the IMM approach. However, unlike an IMM we treat each individual maneuver as a separate hypothesis and use the R-FISST technique to determine

posterior probability of all possible hypotheses. We incorporate FBK by switching from a particle representation of the object PDF to an FBK distribution to determine the OTTA association likelihood. Maneuver uncertainties are handled by tunable noise parameters that describe the direction and magnitude of the change in velocity as well as the initial time and duration of the maneuver.

The rest of the paper is structured as follows. In the following section, we discuss the Fisher-Bingham-Kent distribution (also known as the extreme 5-parameter Fisher-Bingham (FB5e) distribution) that is used to represent the object PDF after maneuver. Next, we briefly discuss the R-FISST framework and how we incorporate the FBK distribution. We then illustrate the theory by applying it to a space object tracking scenario where a single space object can maneuver according to multiple uncertain maneuver models.

2. THE FBK DISTRIBUTION

This section will describe the FBK distribution and will draw from [1] in order to make this paper self-contained. The FBK distribution describes data on the sphere which is unimodal with ellipse-like contours of constant probability. It is particularly suited for data concentrated near an arc of a great circle. The distribution was introduced by Kent et al. [8].

Under this distribution, the probability density of a vector x on the unit sphere $S_2 = \{x \in \mathbb{R}^3 : x^T x = 1\}$, takes the form

$$f(x) = exp\{\kappa y_1 - \delta\, y_3 - c(\kappa, \delta)\} \tag{1}$$

where $\boldsymbol{y} = (\boldsymbol{y_1}, \boldsymbol{y_2}, \boldsymbol{y_3})^{\boldsymbol{T}} = \boldsymbol{R^T x}$ and R is a 3×3 rotation matrix, $R^T R = I_3$ and $|R| = 1$. Note that the R is specified by 3 parameters, which together with $\kappa \geq 0$ and $\delta \geq 0$ comprise the 5 parameters of the distribution. These five parameters are traditionally estimated using maximum likelihood estimates. However, in cases where explicit expressions for the maximum likelihood estimates are unavailable, iterative methods are used to find them. To seed the iterative methods Kent [2] introduces elementary estimates called moment estimates for the parameters of the FBK, $\tilde{R},\ \tilde{\kappa},\ \tilde{\delta}$. Not only are they good for seeding iterative methods these estimates have an explicit representation and are close to the maximum likelihood estimates for the application considered in this paper. This is due to the fact that the typical space object representation falls into the "fully concentrated" category. What it means to be fully concentrated is discussed in more detail later. The following paragraphs give a brief description on how to define the moment estimates [2].

The matrix R is an orientation matrix, which rotates x so that the mode lies in the y_1 direction and such that the y_2 and y_3 form the principal directions of variability, where the variability in the y_2 direction is larger than in the y_3 direction. When starting with a particle cloud representation of the object PDF in Cartesian coordinates, the matrix R can be estimated by a matrix $\tilde{R}$, constructed using the following procedure. First, project the position in Cartesian $x \in \mathbb{R}^3$ coordinates onto the unit sphere such that $x^T x = 1$. Let $\bar{x}$ and **S** be the sample mean vector and the sample dispersion matrix about the zero vector, $\bar{0}$. Let $\bar{\theta}$ and $\bar{\phi}$ denote the latitude and longitude of $\bar{x}$, so that $\bar{x} = [cos\,\bar{\theta}\, cos\bar{\phi}\ , cos\,\bar{\theta}\, sin\bar{\phi}\ , sin\,\bar{\theta}\ ]^T$. Choose an orthogonal matrix **C** to rotate $\bar{x}$ s.t. $\boldsymbol{C^T}\bar{x} = [1,0,0]^T$; for example,

$$\boldsymbol{C} = \begin{bmatrix} cos\,\bar{\theta}\, cos\,\bar{\phi} & -sin\,\bar{\phi} & -sin\,\bar{\theta}\, cos\,\bar{\phi} \\ cos\,\bar{\theta}\, sin\,\bar{\phi} & cos\,\bar{\phi} & -sin\,\bar{\theta}\, sin\,\bar{\phi} \\ sin\,\bar{\theta} & 0 & cos\,\bar{\theta} \end{bmatrix}. \tag{2}$$

The next step is to choose a rotation **K** that diagonalizes the lower right (2×2) of $\boldsymbol{B} = \boldsymbol{C^T S C}$. The rotation matrix **K** can be selected using the elements of **B**,

$$\boldsymbol{K} = \begin{bmatrix} 1 & 0 & 0 \\ 0 & cos\bar{\psi} & -sin\bar{\psi} \\ 0 & sin\bar{\psi} & cos\bar{\psi} \end{bmatrix}', \tag{3}$$

where

$$tan\, 2\bar{\psi} = (2b_{23})/(b_{22} - b_{33}). \tag{4}$$

This is done to ensure that the following conditions hold when $\bar{y} = \tilde{R}^T \bar{x}$ and $T = \tilde{R}^T \boldsymbol{S} \tilde{R}$:

$$\bar{y}_2 = \bar{y}_3 = 0, \quad \bar{y}_1 > 0, \quad T_{23} = 0 \quad T_{22} > T_{33} \tag{5}$$

Ensuring these conditions hold the matrix $\tilde{R}$ is then $\tilde{R} = \boldsymbol{CK}$. The other two moment estimates can be explicitly approximated:

$$\tilde{\kappa} = \frac{1}{T_{22}}, \tag{6}$$

$$\bar{\delta} = \frac{1}{2}\left(\frac{1}{T_{33}} - \frac{1}{T_{22}}\right). \tag{7}$$

These approximations for $\tilde{\kappa}$ and $\bar{\delta}$ are known as the asymptotic moment estimators. Also, note that

$$\frac{1}{\bar{\kappa}} = T_{22} \approx var(y_2) \approx var(\phi), \qquad \phi = longitude,$$
$$\frac{1}{\bar{\kappa} + 2\bar{\delta}} = T_{33} \approx var(y_3) \approx var(\theta), \qquad \theta = latittude.$$

The log normalizing constant *c (κ, δ)* is chosen so that the integral of *f(x)* over the unit sphere (with respect to the uniform measure) equals one. So far there is no simple general explicit form for *c (κ, δ)*. However, progress can be made in two special cases: the semi-concentrated case where κ+2δ is large and κ is small or moderate; and the fully-concentrated case where both κ and κ+2δ are large. In both cases explicit approximate formulas for *c (κ, δ)* are available. As a rough rule of thumb, we can say that κ + 2δ is large if it exceeds 20, and that κ is large if it exceeds 20, though it should be possible to relax these thresholds. For many space object applications the level of uncertainty falls within the fully concentrated case; occasionally the semi-concentrated case is appropriate when propagating uncertainty several orbits into the future [8].

For a unit vector $\boldsymbol{y} = (\boldsymbol{y_1}, \boldsymbol{y_2}, \boldsymbol{y_3})^{\boldsymbol{T}}$ the latitude θ ∈ [−π/2, π/2] and the longitude φ ∈ [−π, π] can be defined

$$\boldsymbol{y_1} = cos\theta\, cos\phi, \quad \boldsymbol{y_2} = cos\theta\, sin\phi, \quad \boldsymbol{y_3} = sin\theta$$

In the semi-concentrated case (κ small or moderate and κ + 2δ large), the distribution is concentrated near the equator $\boldsymbol{y_3} = \boldsymbol{0}$. In terms of polar coordinates, ϕ and θ are approximately independent where ϕapproximately follows a von Mises distribution on the circle, with density

$$f(\phi) \propto exp\{\kappa\, cos\phi\} \tag{8}$$

and where θ approximately follows a normal distribution, with density

$$f(\theta) \propto exp\{-\frac{1}{2}(\kappa + 2\delta)\theta^2\} \tag{9}$$

In the fully concentrated case (both κ and κ + 2δ large), $\boldsymbol{y_2}$is also near 0 and the von Mises distribution is approximately normal,

$$f(\phi) \propto exp\{-\frac{1}{2}\kappa\phi^2\} \tag{10}$$

For the purposes of this paper we focus on the fully-concentrated case. Using equations (9)– (10), the approximate joint density of θ and φ reduces to the bivariate normal density

$$f(\theta, \phi) = \frac{\sqrt{\kappa(\kappa+2\delta)}}{2\pi} exp\{-\frac{1}{2}(\kappa\phi^2 + (\kappa + 2\delta)\theta^2)\} \tag{11}$$

so that $\phi \sim N(0, 1/\kappa)$ independent of $\theta \sim N(0, 1/(\kappa + 2\delta))$.

3. FBK WITHIN R-FISST

In this section, we discuss how we incorporate the FBK data association into the Finite Set Statistics (FISST) Bayesian Recursions. Randomized Finite Set Statistics is a multiple object tracking technique that approximates the computationally intractable FISST Bayesian recursions. The technique uses a hypothesis dependent derivation of the FISST equations which allows for a randomized scheme that samples the highly probable hypotheses to keep the multi-object tracking problem tractable. Within R-FISST there are no assumptions on the form of the object PDF. The derivation allows one to break down the posterior distribution into two terms that are linked by a likelihood term. For the full derivation and applications please see [9,10]. For the sake of brevity, we only discuss the portions of the R-FISST derivations necessary to discuss the FBK implementation. To incorporate the FBK data association into R-FISST we convert the object PDF to an FBK distribution after we receive angles only measurements in form of right ascension and declination. Given an object PDF $p(X)$ where X is a d-dimension state vector that the object occupies. The PDF $p(X)$ is typically represented by a particle ensemble in the R-FISST framework to better account for the non-linearities in propagation and avoid Gaussian assumptions that typically become non-Gaussian through propagation and update. Through sampling the PDF, we represent the PDF using the set of d-dimension state vectors $\{x_1, x_2, \dots, x_{NP}\}$ where x_j is a single particle sample of the PDF and $j = 1, 2, \dots, N_p$. In this representation the number of samples, N_p, must always be sufficient to accurately capture the statistics of the PDF. Using these samples, we determine the parameters, $R, \kappa, \delta,$ of the corresponding FBK distribution using the steps provided in the previous section. Then given a measurement, z, on the sphere which may come from any of the, J, predicted PDF, with FBK densities $f_j(z),\ j = 1,2,..J$, within a hypothesis we calculate the FBK posterior and use it in place of the weight for the predicted hypothesis. Given that all are equally likely the posterior will take the form,

$$p_j(z) = \frac{f_j(z)}{\sum_k^J f_k(z)}.\quad j = 1, \dots, J \tag{12}$$

Where $f(z)$ is from the equation (12). This value will be used in the R-FISST Bayesian recursions to determine the likely hypotheses.

4. TRACKING A MANEUVERING RSO

In this section, we apply the R-FISST technique coupled with FBK data association to a space object tracking problem in which a single RSO maneuvers according to one of four different maneuvers. The example is of a GEO RSO with orbital parameters according to Table 1. The RSO is tracked using an optical sensor with observation error noise, assumed zero-mean Gaussian with a standard deviation of 2 $arcseconds$ in both right ascension and declination. Within the simulation the expected optical measurements will suddenly no longer correlate to the RSO signaling a possible maneuver. Observations are received in ten-minute intervals. It will be assumed that the object under went one of the four typical maneuvers that adjust the RSO position in the θ and ϕ directions. In the following analysis, we attempt to discern which maneuver occurred (if any) in an environment with large maneuver uncertainties as well as maintain accurate estimations of the RSO throughout the simulation. We do this by creating a maneuver hypothesis for each maneuver and maintain these hypotheses using the R-FISST technique.

Element	Value
Semi-Major axis, a	42111123.663 (m)
Eccentricity, e	0.039907 (rad)
Inclination, i	0.0017450 (rad)
Argument of Perigee, ω	2.5587×10−5 (rad)
Right Ascension of Ascending Node, Ω	3.5079 (rad)
True Anomaly, ν	6.0153 (rad)

Table 1. RSO Orbital Elements

The scenarios are simulated using Scala with Eclipse IDE on a Dell Precision7510. The RSO was propagated using Orekit numerical orbit propagation with the Homes Featherstone attraction model. The maneuvers were modeled using Orekit's analytical maneuver tool kit with assumed zero mean Gaussian noise in maneuver pointing direction,

maneuver velocity increment, and engine specific impulse with 1×10^{-2} meters, ten meters per second, and 1×10^{-2} seconds standard deviation. Process noise is increased at the time of expected maneuver to account for uncertainty in the maneuver time and duration assumed to be zero mean Gaussian with five-thousand meters standard deviation in position and one kilometer per second in velocity.

We consider two scenarios to better illustrate the utility of FBK data association for tracking maneuvering objects within the R-FISST framework. In both scenarios, the true object performs maneuver number two. Also, for the provided time windows of all figures the object is within the field of view (FOV) of the sensor. The first simulation, Case 1, is an example of what happens when no maneuver modeling is performed. The second simulation, Case 2, uses the techniques discussed above. Fig. 1 shows the results of tracking the object without using the maneuver hypotheses coupled with the FBK for data association. In Fig. 1, the y-axis shows the rank of the weights of the hypotheses. The higher the rank,

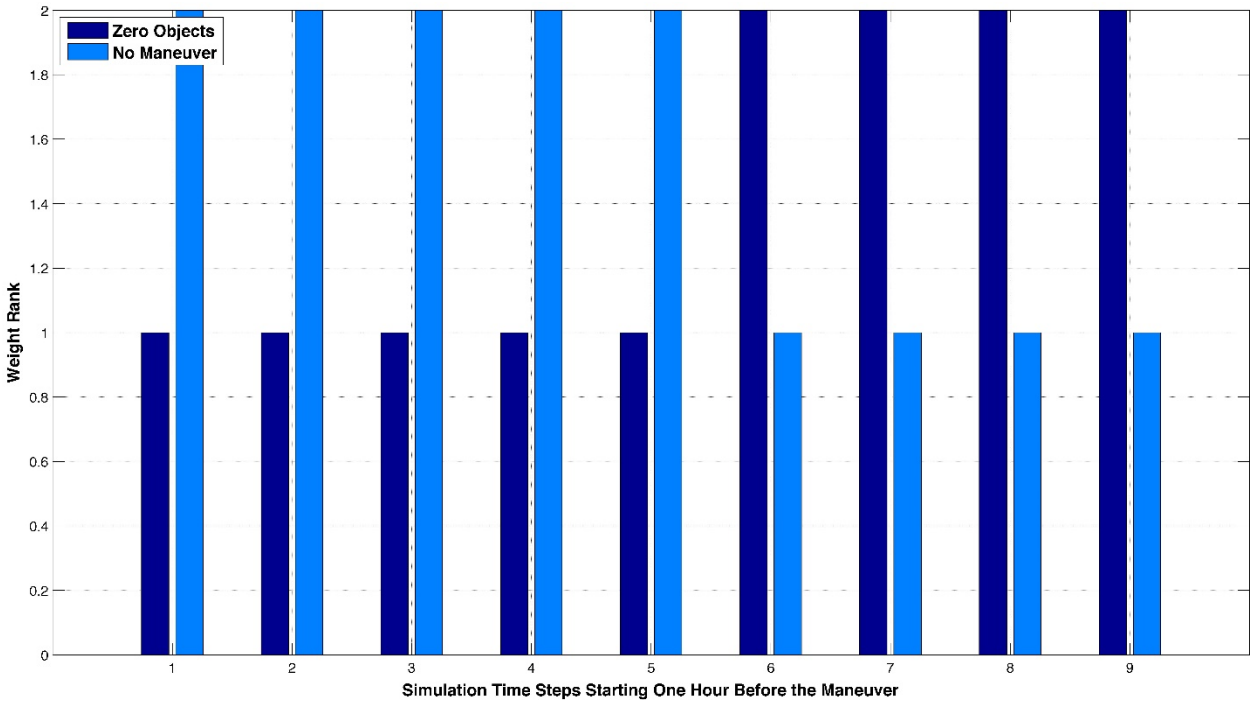

Fig. 1. Ranks of the weights of the two hypotheses vs. simulation time starting one hour before the maneuver for Case 1. Custody is lost due to the maneuver. Before the maneuver (before step six) the hypothesis containing one object (light blue, "No Maneuver") had the highest rank, After the maneuver (after time step six) the hypotheses with zero objects (dark blue) has the highest rank signaling a loss of custody.

the more the hypothesis weighs. The x-axis shows the simulation time steps starting one hour before the maneuver. The figure illustrates that without maneuver hypotheses the custody of the RSO will be lost. The zero-object hypothesis has more weight after the maneuver signifying an incorrect belief that there are no objects. Fig. 2 shows the results of the approach discussed in this paper. Instead of having two hypotheses as in Fig. 1 There are now six hypotheses: one for each of the four maneuvers, another for the case where the object does not maneuver, and lastly one for the zero-object hypothesis. In Fig. 2 at each time step before the maneuver the maneuvering hypotheses are equally ranked the lowest. However, after the maneuver in step six the hypothesis containing the object that performed maneuver number two has the most weight. This corresponds with the true maneuver showing that the FBK data association likelihood correctly associated and tracked the maneuvering object.

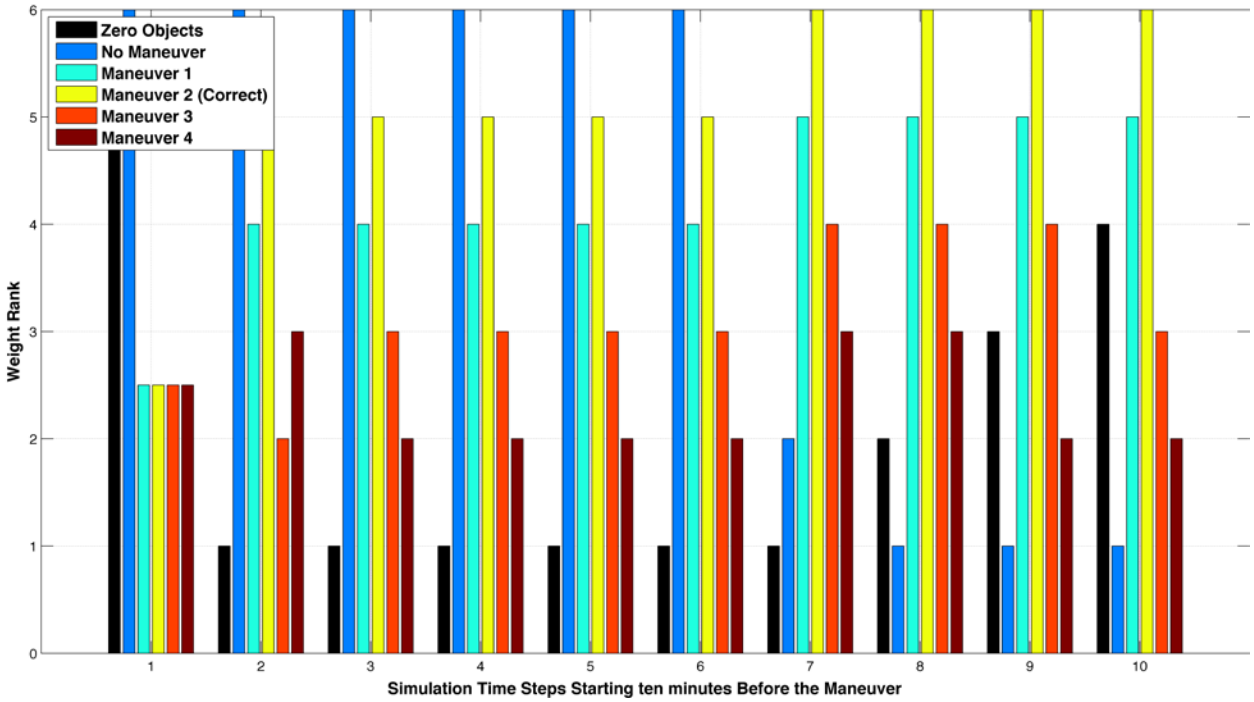

Fig. 2. The rank of the weights of all six hypotheses for Case 2. After the maneuver, the hypothesis corresponding to maneuver two has the highest rank which correlates to the true maneuver. This signifies that the methods provided within could track the correct maneuver and maintain object custody.

The above results are further exemplified by considering the total entropy as discussed in [10]. The total entropy, S_{tot}, is a measure of the uncertain within a hypothesis. For our purposes, we analyze the total entropy of the hypothesis with the highest weight to show that as measurements are received the uncertainty is decreasing. The total entropy is,

$$S_{tot} = \sum_{l=1}^{M} S_l = \frac{1}{2}\sum_{l=1}^{M} log(|P_l|\,(2\pi e)^N), \tag{13}$$

where P_l is the LU factorization of the ensemble covariance of the particle cloud representation of the object PDF. The variable, N, is the dimension of the covariance. The variable, M, is the number of objects within the top hypothesis. In the considered scenarios M will either be one or zero. The results from the first scenario in which the object is lost are shown in Fig. 3. The y-axis of Fig. 3 is the total entropy and the x-axis represents the simulation time steps. Before the maneuver, measurements are being received and the entropy is decreasing. After the maneuver, there is a sudden drop to zero entropy signifying loss of custody. The results for the case where object custody is maintained are shown in Fig. 4. Therein, before the maneuver the trend of entropy is decreasing as in Fig. 3. However, after the maneuver there is a spike in entropy that is associated with the high uncertainties involved in the maneuver prediction. After the initial spike, the entropy begins to trend downward again. This is significant for two reasons: 1) It shows that a maneuvering hypothesis has become the most probable hypothesis, 2) It shows that the highest probable hypothesis is continuing to associate with the maneuvered object.

Lastly, Fig. 5 illustrates the cumulative number of “false positives” and “false negatives” for both cases. In this case let’s say a false positive, also known as a type one error, is an occurrence where evidence was falsely associated to the wrong maneuver type. A false negative, also known as a type two error, is the case where the belief is that there was no maneuver when there was. In Fig 5. the y axis represents the sum of all false positives and negatives. The x-axis is the simulation time steps after the maneuver. The first case, is represented by the black line and grows linear with time. The second case grows linear through the first four time steps due to false negatives caused by the ambiguity just after maneuver is applied. It then levels out with only one other false positive.

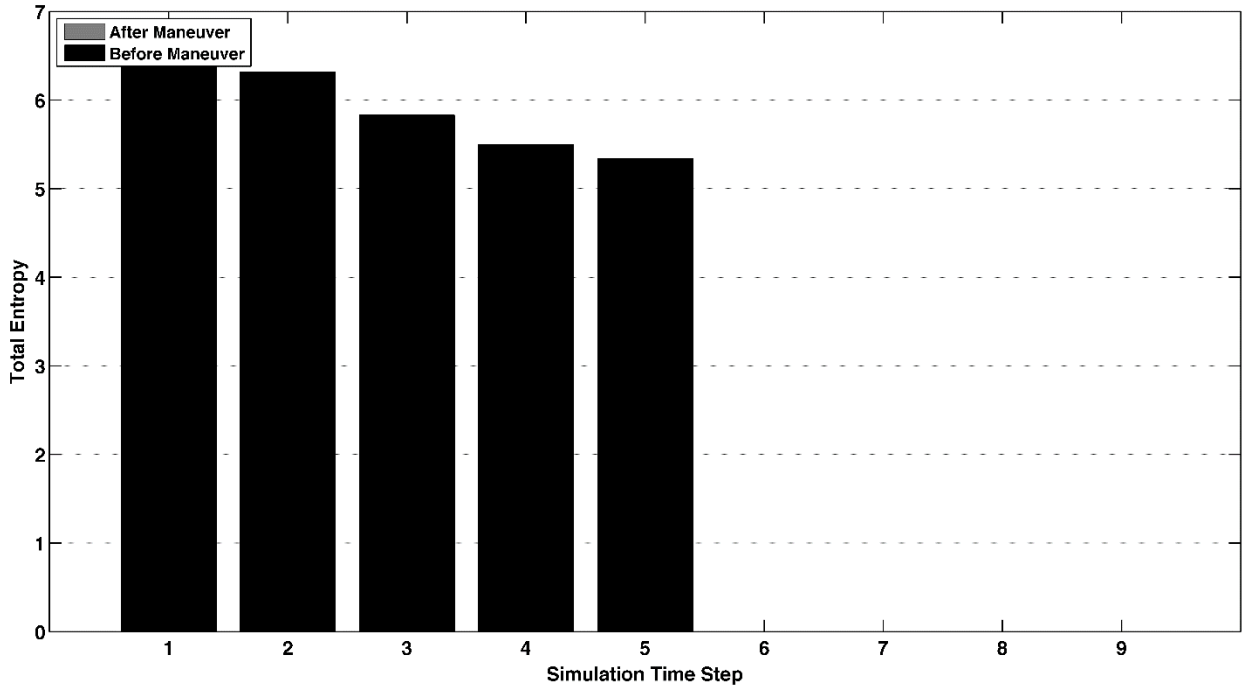

Fig. 3. Total Entropy of the most probable hypothesis throughout time in Case 1. The sudden drop in entropy after the maneuver signifies a loss of custody.

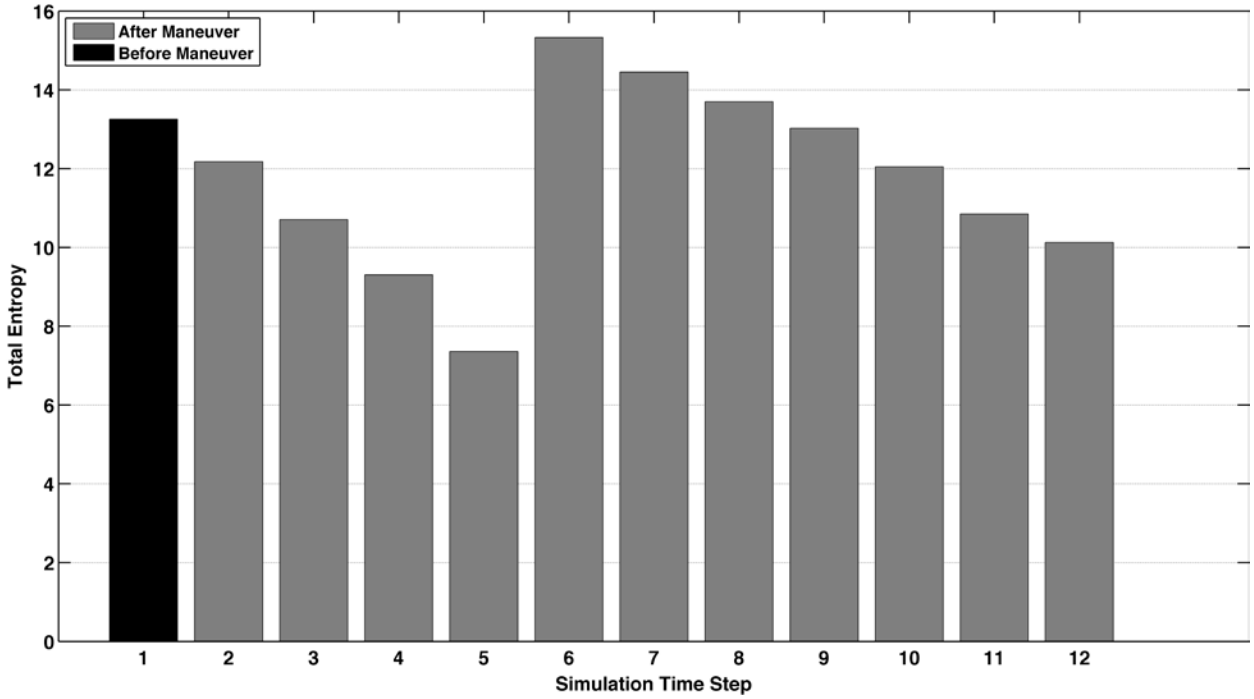

Fig. 4 Total Entropy of the most probable hypothesis throughout time in Case 2. Custody of the maneuvering object is maintained.

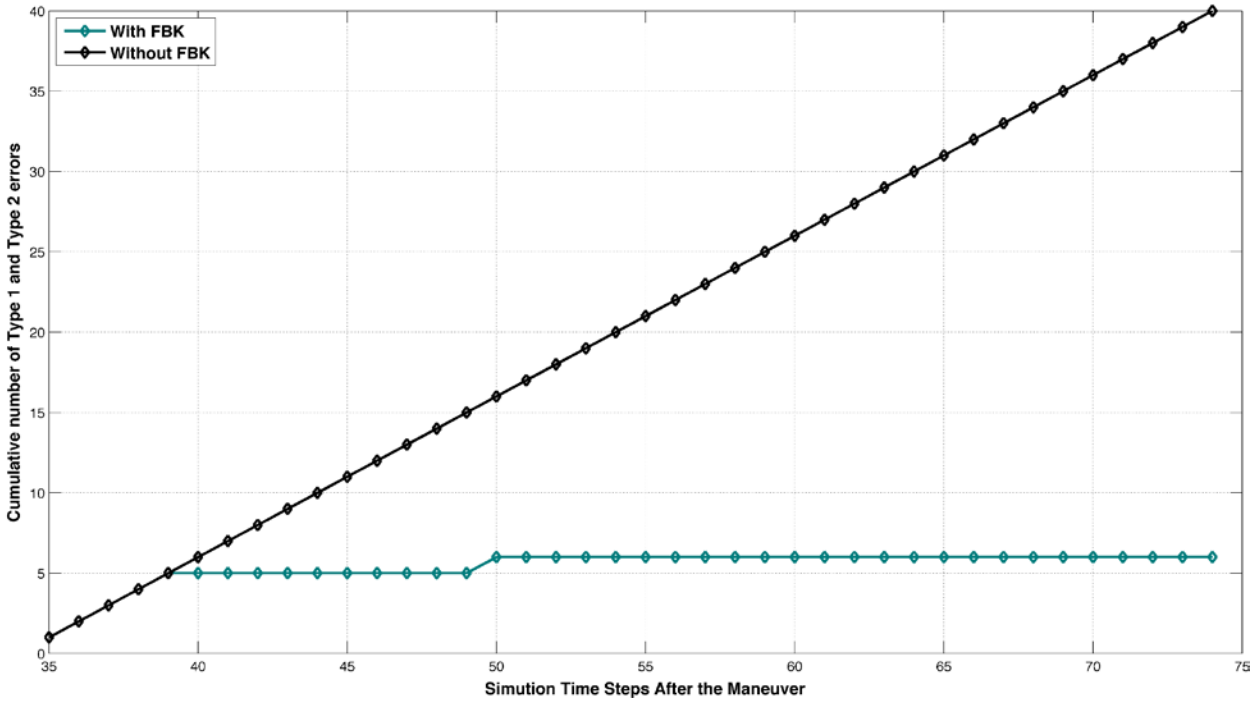

Figure 5. The cumulative number of false positives and false negatives for each case.

5. CONCLUSIONS

In this paper, we have provided a description of the FBK distribution and its use in determining association of angles-only optical measurements to maneuvering objects. Most often in SSA the space object uncertainty will fall into a classification called "fully-concentrated" for which explicit expressions for FBK approximations are known. As illustrated in the results section, losing object custody can lead to false beliefs in object location as well as incorrect assumptions of the number of objects. Using the FBK distribution coupled with the R-FISST multi-object tracking approach we showed the capability of maintaining custody of a maneuvering GEO RSO. The maneuver uncertainties considered included: uncertainty in the object state at the time of maneuver, the direction of the maneuver, the magnitude of the maneuver impulse, the direction of the maneuver impulse, the time of the maneuver, and the duration. This paper provides a platform for future work, which includes providing tractable solutions to the maneuvering object tracking problem in all orbit regimes as well as displaying results of tracking multiple maneuvering objects within a clutter filled environment.

6. ACKNOWLEDGEMENTS

This material is based upon work supported by the Air Force Office of Scientific Research, Air Force Material Command, USAF under Award No. FA9550-16-1-0099.

7. REFERENCES

1 W.R. Faber, I. I. Hussein, J. T. Kent, S.Bhattacharjee, and M.K.Jah "Optical Data Association in a Multi-Hypothesis Framework with Maneuvers" AAS/AIAA Astrodynamics Specialist Conference Columbia River Gorge, Stevenson, WA. August 2017. 17-639

2 J. T. Kent, "The Fisher-Bingham distribution on the sphere," Journal of the Royal Statistical Society, Series B, Vol. 44, 1982, pp. 71–80.

3 J. T. Kent, S.Bhattacharjee, I.Hussein, and M.K.Jah, "Angles-Only Data Association Using Directional Discriminant Analysis," 2016. Space Flight Mechanics Meeting San Antonio, Texas.

4 B. Jia, K. D. Pham, E. Blasch, D. Shen, Z. Wang, X. Tian, and G. Chen, "Space object tracking and maneuver detection via interacting multiple model cubature Kalman filters," Proceedings of the IEEE Aerospace Conference, 2015.

5 B. Chen and J. K. Tugnait, "Tracking of multiple maneuvering targets in clutter using IMM/JPDA filtering and fixed-lag smoothing," Automatica, Elsevier, February 2001.

6 J. Siminski, T. Flohrer, and T. Schildknecht, "Assessment of Post Maneuver Observation Correlation Using Short-Arc Tracklets," 7th European Conference on Space Debris, April 18-21, 2017.

7 W. R. Faber., S. Chakravorty, Ph.D., and Islam I. Hussein, Ph.D. Multiple Space Object Tracking with R-FISST. Proc. of AAS/AIAA Space Flight Mechanics Meeting, Texas, San Antonio. 2017

8 J. T. Kent, I. Hussein, and M. K. Jah, "Directional Distributions in Tracking of Space Debris," Proceedings of the 19th International Conference on Information Fusion (FUSION), Heidelberg, Germany, IEEE, 2016.

9 W. Faber, S. Chakravorty, and I. Hussein, "R-FISST and the Data Association Problem with Applications to Space Situational Awareness," AIAA Space and Astronautics Forum and Exposition, September 2016

10 W. R. Faber, W. Zaidi, I. Hussein, C. W. T. Roscoe, M. P. Wilkins, and J. Paul W. Schumacher, "Application of Multi-Hypothesis Sequential Monte Carlo For Breakup Analysis," 2017. (Proceedings of the AAS/AIAA Astrodynamics Specialist Conference, Columbia River Gorge, Stevenson, WA Paper AAS 17-579).